Singlet Fission in 9,10-Bis(phenylethynyl)anthracene Thin Films

Youn Jue Bae, Gyeongwon Kang, Christos D. Malliakas, Jordan N. Nelson, Jiawang Zhou, Ryan M. Young, Yi-Lin Wu, Richard P. Van Duyne, George C. Schatz, and Michael R. Wasielewski*

Department of Chemistry and Institute for Sustainability and Energy at Northwestern, Northwestern University, Evanston, Illinois 60208-3113, United States

* Supporting Information

ABSTRACT: Singlet fission (SF) in two or more electronically coupled organic chromophores converts a high-energy singlet exciton into two low-energy triplet excitons, which can be used to increase solar cell efficiency. Many known SF chromophores are unsuitable for device applications due to chemical instability and low triplet state energies. The results described here show that efficient SF occurs in polycrystalline thin films of 9,10-bis(phenylethynyl)anthracene (BPEA), a commercial dye that has singlet and triplet energies of 2.40 and 1.11 eV, respectively, in the solid state. BPEA crystallizes into two polymorphs with space groups C2/c and Pbcn, which undergo SF with $k_{SFA} = (109 \pm 4\ ps)^{-1}$ and $k_{SFB} = (490 \pm 10\ ps)^{-1}$, respectively. The high triplet energy and efficient SF evidenced from the 180 ± 20% triplet yield make BPEA a promising candidate for enhancing solar cell performance.

Singlet fission (SF), the process by which a singlet exciton created in an assembly of two or more interacting chromophores energetically down-converts into two triplet excitons, was first discovered in 1965 in crystalline anthracene.[1] Over the past decade, SF chromophores have attracted renewed attention because of their ability to overcome the Shockley−Quiesser limit on the theoretical efficiency of single-junction solar cells.[2,3] Specifically, SF chromophores can mitigate thermalization losses, where the absorbed photon energy in excess of the band gap is lost to heat.[4] The triplet excitons can be harvested by either energy transfer or charge transfer to ultimately create charge carriers.[5,6] For example, Dexter-type[7] energy transfer from triplet excitons of pentacene and tetracene to lead-based quantum dots has been demonstrated.[8,9] Charge transfer from the triplet exciton is also possible if the SF chromophores are paired with a suitable electron acceptor or donor, following the architecture of conventional organic solar cells.[10,11] According to detailed balance, the maximum theoretical efficiency for a single-junction photovoltaic cell is achieved with a band gap of 1.1−1.3 eV.[12] Thus, the triplet energy of a SF chromophore incorporated into a photovoltaic device should be >1.1 eV. In addition, because Frenkel excitons in organic chromophores have large binding energies, higher triplet energies facilitate charge transfer to a nearby donor or acceptor.[13]

9,10-Bis(phenylethynyl)anthracene (BPEA) is a robust, industrial dye that has been widely used for chemiluminescent lighting,[14−16] photoswitches,[17] optical waveguides[18] and solar cells.[19] Its good chemical and thermal stabilities along with its facile synthesis and functionalization allow a wide range of different photochemical and photophysical applications.[20] BPEA is a strong blue light absorber with a near unity quantum yield (Φ_f = 1) of green fluorescence.[21] Various structural modifications of BPEA have been reported and highlight its tunable electronic properties.[15,22] Although BPEA has been suggested as a potential SF candidate,[2] only one study of SF in BPEA nanoaggregates has appeared following submission of this manuscript.[23] Moreover, a recent report on 9,10-bis(TIPS)anthracene aggregates in solution showed only modest SF yields.[24] Crystalline BPEA powder obtained from Sigma-Aldrich contains 59.90 ± 0.02% C2/c and 40.10 ± 0.02% Pbcn polymorphs (Figure 1a) based on a quantitative powder X-ray diffraction (PXRD) analysis (Figure S1).[17] BPEA films were prepared by thermal vapor deposition under high vacuum onto a sapphire substrate followed by two annealing methods: solvent vapor annealing with dichloromethane for 12 h or thermal annealing at 120 °C for 3 h. Samples for PXRD analysis were scraped off the annealed films to remove preferred orientations. Analysis of the PXRD data (Figure 1b) using full-profile Rietveld fitting[25] against the two reported crystal structures of BPEA[17,26] reveals that the solvent-annealed film contains 61.2 ± 0.5% of the C2/c and 38.8 ± 0.5% of the Pbcn polymorphs, while the thermally annealed film contains >97% of the Pbcn polymorph.

BPEA in solution has a 2.64 eV S_1 state energy, Φ_f = 1, and a 3.17 ± 0.02 ns S_1 lifetime (Figure S2).[27] In both the solvent- and thermally annealed films, the S_1 energy decreases to 2.40 eV (Figure 2), which is expected from transition dipole−dipole coupling and orbital overlap-driven electronic coupling among chromophores.[28] The fluorescence of both the solvent and thermally annealed films is significantly quenched to Φ_f = 0.04 ± 0.01 and 0.27 ± 0.04, respectively. BPEA phosphorescence in glassy 2-methyltetrahydrofuran at 77 K is essentially undetectable because of its extremely low spin−orbit-induced intersystem crossing quantum yield (10^{-5}).[20] Even in thin films where a significant triplet population is formed (vide infra), phosphorescence is undetectable at 77 K. Thus, we used palladium octabutoxyphthalocyanine, $PdPc(OBu)_8$, which has

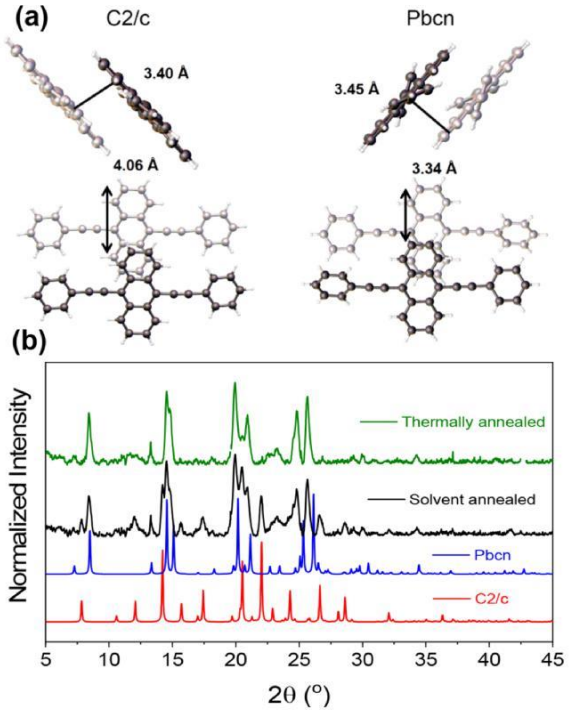

Figure 1. (a) BPEA dimer from the crystal structure of the C2/c (left) and Pbcn (right) polymorphs. (b) Comparison of the simulated PXRD patterns of the C2/c (red) and Pbcn (blue) polymorphs with the PXRD pattern of the solvent-annealed (black) and the thermally annealed (green) BPEA thin films.

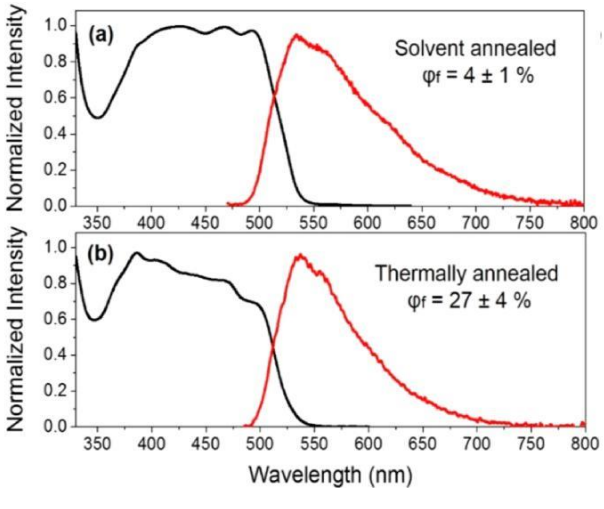

Figure 2. Steady-state absorbance (black) and emission (red) spectra of (a) solvent-annealed (b) thermally annealed polycrystalline BPEA thin films.

a 1.24 eV triplet state energy, as a photosensitizer to produce the BPEA triplet state in a film.[29,30] Following selective photoexcitation of $PdPc(OBu)_8$ at 720 nm (Figure S3), rapid intersystem crossing populates ^{3}*$PdPc(OBu)_8$, which then energy transfers to BPEA to produce ^{3}*BPEA (Figure S4). This observation places an upper bound on the ^{3}*BPEA energy as $E(T_1) \leq 1.24$ eV in the solid film. In addition, the observation of delayed fluorescence (Figure S6) from the photoexcited solvent-annealed film indicates that the ^{3}*BPEA energy must be close to 1.20 eV, which is half the S_1 energy, 2.40 eV. Observation of singlet oxygen emission at 0.98 eV (Figure S7) gives the lower limit and based on these data, $E(T_1) = 1.11 \pm 0.13$ eV, so that SF in the BPEA film should be nearly isoergic, and somewhat slower than for exoergic polyacenes.[31,32] However, efficient SF is observed even in films of endoergic chromophores.[33–35]

Figure 3 shows the femtosecond transient absorption (fsTA) spectra of the solvent-annealed 170 nm BPEA film following

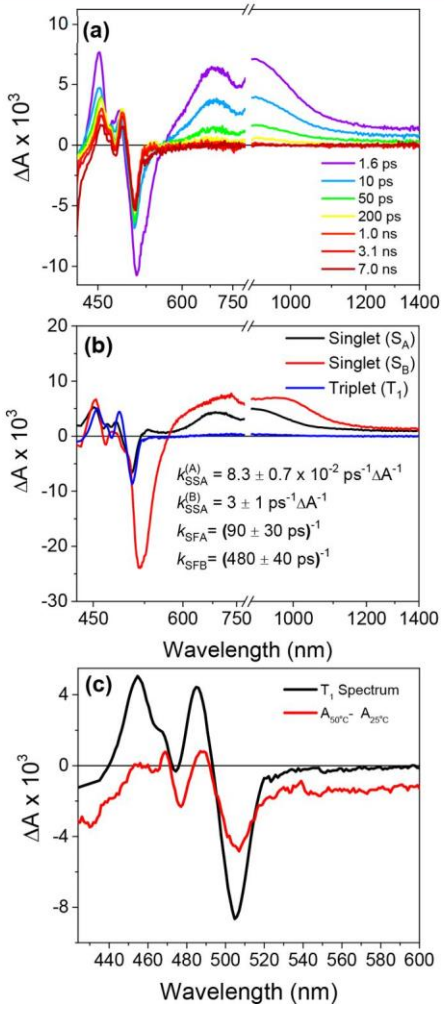

Figure 3. (a) FsTA spectra of a solvent-annealed 170 nm BPEA film using (a) 414 nm, 100 fs, 1 kHz laser pulses, (b) species-associated spectra and rate constants and (c) comparison of the transient difference spectrum of the triplet state to the thermal difference spectrum. Wavelengths for panels b and c are shown in reciprocal space to highlight the blue region of the spectrum. Reported values are the average and std. deviation from multiple experiments.

excitation with a 414 nm, 100 fs laser pulse at a 1 kHz repetition rate and an excitation density of 7.8×10^{19} cm^{-3}. The transient spectrum (Figure 3a) at early times exhibits ground-state bleaching (GSB) overlapped with stimulated emission (SE) near 420 and 550 nm, which is consistent with the steady-state absorption and emission spectra (Figure 2), and $S_n \leftarrow S_1$ excited-state absorption (ESA) features from 550 to 1400 nm, which are broadened compared to those in solution (Figure S2b). At later times, the ESA at 445–495 nm is assigned to $T_n \leftarrow T_1$ absorption based on the triplet-sensitized spectrum (Figures S4 and S5) with an overlapping GSB feature at 495–550 nm. The kinetic fits and species

populations are shown in Figure S8. In order to distinguish the triplet spectrum from the thermally induced spectral shift in the ground state bleach,[36] we compared the species-associated triplet spectrum to the ground state thermal difference spectrum between 50 and 25 °C (Figure 3c). Although the similar spectral shape indicates that there is some degree of thermal effect present, the magnitude is smaller than the observed $T_n \leftarrow T_1$ spectrum and the overall A of the thermal spectrum is negative. In addition, singlet oxygen emission (Figure S7) supports formation of triplet in the thin film and the polymorph-dependent triplet yield suggests that A at later pump−probe delays results from the triplet. Similar spectra are obtained for the thermally annealed 310 nm BPEA film, except that the SE feature is dominant (Figure S9a). Since the initial rapid decay of the GSB and $S_n \leftarrow S_1$ ESA imply that singlet−singlet annihilation (SSA) occurs at the excitation density used,[31,32] the data were globally fit using a kinetic model that includes SSA and the relative polymorph populations (see SI) to yield $k_{SFA} = (90 \pm 30\ ps)^{-1}$ and $k_{SFB} = (480 \pm 40\ ps)^{-1}$ for the two BPEA polymorphs. Similar values are obtained using fsTA and picosecond time-resolved fluorescence (TRF) systems having 100 kHz repetition rates with excitation densities of 10^{17} and 10^{16} cm^{-3}, respectively. (Figures S10−S13). TRF spectroscopy was also used to obtain the triplet−triplet annihilation rate constant $k_T = (196 \pm 5\ ns/A)^{-1}$ responsible for the delayed fluorescence (Figure S6b).

As shown in the PXRD pattern (Figure 1), the thermally annealed film is more than 97% Pbcn polymorph, which permits a straightforward assignment of the two observed SF rates. Picosecond TRF spectra of the thermally annealed film (Figures S14 and S15) were globally fit to yield $k_{SFB} = (490 \pm 10\ ps)^{-1}$. Thus, the slower SF rate results from the Pbcn polymorph, while the faster SF rate derives from the C2/c polymorph.

Nanosecond transient absorption (nsTA) spectra (Figure S16) of the BPEA films were employed to determine their triplet yields using the singlet depletion method,[37] which has been demonstrated to be effective in obtaining SF yields (Figures 4, S15, Table S1).[34,38−40] The number of excited molecules was calculated from the excitation pulse energy, laser spot size, and film thickness to obtain the expected ground-state bleach spectrum; then, the number of triplet states was estimated by adding the scaled ground-state bleach to the transient absorption spectrum of the solvent-annealed BPEA film. For the solvent-annealed BPEA film, 100% of the expected bleach was needed to remove the negative transient spectra features at 52 ns (Figure 4). By correcting for the triplet decay experienced by 52 ns, the time-independent triplet yield extrapolated to 1.5 ns, when SF is essentially complete, is 180 ± 20% (see SI). A similar procedure applied to data for the thermally annealed BPEA film gives an 80 ± 20% triplet yield (Figure S17). Application of the spectral deconvolution method gives similar values for the triplet yield (Figure S18).

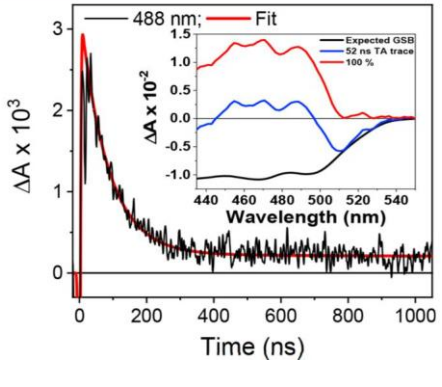

Figure 4. Triplet−triplet absorption decay of the solvent-annealed BPEA film ($\tau_1 = 80 \pm 10$ ns (94%); $\tau_2 > 4$ μs (6%) following 416 nm, 7 ns pulses at 10 Hz. Inset: the triplet−triplet absorption spectrum determined from the nsTA spectrum at 52 ns using the singlet depletion method.

In order to understand the origin of the SF rate difference between the two polymorphs, we compared the detailed structures of the dimer units in the crystal structure and calculated their effective electronic couplings.[31,35,41] Among the three different neighboring dimers of each polymorph (Figures S19−S21), Figure 1a shows the dimer that has the largest electronic coupling (Tables S3 and S4). Comparing the packing between the two dimer units from each polymorph, both have the same 0.80 Å longitudinal slip distance, and similar π−π distances, 3.40 Å for C2/c and 3.45 Å for Pbcn. The largest structural difference between the dimer units occurs in the lateral slip distances, which are 4.06 Å for C2/c and 3.33 Å for Pbcn. Such differences change orbital overlap, resulting in different effective electronic coupling between the two polymorphs.

Considering the first-order coupling of CT states to the initially excited singlet state, $^1(S_0S_1)$, and the final correlated triplet pair state, $^1(T_1T_1)$, the effective electronic coupling for the superexchange mechanism, $J_{SE,eff}$, was calculated using eq 1:[42]

$$J_{SE,eff} = \langle {}^1S_1S_0 | \hat{V} | {}^1T_1T_{11} \rangle = \langle S_1S_0^0 | \hat{H}_{el} | TT_{11}^0 \rangle - \frac{2(V_{LL}V_{LH} - V_{HH}V_{HL})}{[E(CT) - E(TT)] + [E(CT) - E(S_1)]} \quad (1)$$

The first term on the right-hand side of the equation will be ignored because the direct two-electron coupling is small compared to the four one-electron couplings.[43] V_{LL} and V_{HH} are the one-electron couplings of the LUMO and HOMO of the two molecules, respectively, whereas V_{LH} and V_{HL} are one-electron couplings between the LUMO of the first molecule and the HOMO of the second molecule, and vice versa. Using the values specified in Tables S3 and S5 (see the SI for computational details), $J_{SE,eff}$ is 3.73 meV for Pbcn and 7.80 meV for C2/c. Assuming the reorganization energies are similar for both polymorphs, and since the SF rate is proportional to $|J_{SE,eff}|^2$, the SF rate for C2/c is estimated to be 4.4 times faster than that of Pbcn. The large $J_{SE,eff}$ value for the C2/c polymorph is mainly due to the significant LUMO−LUMO coupling, V_{LL}, which is 120 meV for C2/c and 11.7 meV for Pbcn (Table S4). This large LUMO−LUMO coupling is also visualized in the molecular orbital diagrams shown in Figure S22, where the electron density of the LUMO is mainly localized on the anthracene. The spatial overlap of the LUMOs of the C2/c dimer is larger than that of the Pbcn dimer, resulting in energy splitting of the degenerate LUMOs.

It is widely known that the slip distance is an important factor in determining SF rates.[43−46] In order to understand the effect of lateral slip distance (X), the effective electronic coupling and the one-electron couplings were calculated with the fixed π−π and longitudinal slip distances of the C2/c

polymorph, where X is varied (Figure 5). The value of $|J_{SE,eff}|^2$ for the C2/c polymorph decreases as X increases from 3.0

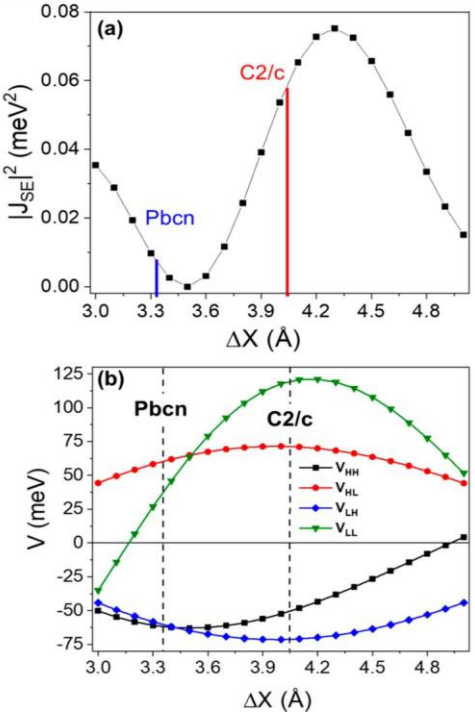

Figure 5. (a) Calculated effective electronic coupling constant $J_{SF,eff}$ vs lateral slip distance X and (b) the 1-electron couplings V_{LL}, V_{LH}, V_{HH}, and V_{HL} vs lateral slip distance (X) using the C2/c polymorph π−π and longitudinal slip distances.

to3.5 Å, then increases and peaks at 4.3 Å (Figure 5a). Thus, we know that the lateral slip distance is a major factor influencing the difference in the electronic couplings between the two polymorphs. Among the four one-electron couplings, V_{LL} changes most drastically in respect to X (Figure 5b) indicating that LUMO−LUMO coupling primarily determines the overall SF rate in BPEA.

The SF rate ratio between the C2/c and Pbcn polymorphs obtained from experiment is 4.5 ± 0.2, while that from the computations is 4.4, and are therefore in very close agreement, indicating that simple electronic coupling calculations of the dimer unit can provide useful information regarding SF dynamics; however, caution should be taken since the dimer model does not entirely represent the thin film system and has shown to fail in predicting polymorph dependent SF in tetracene system.[47] Our results show that the lateral slip distance in BPEA is a significant factor determining SF dynamics; thus, in future work we will improve the effective coupling between the BPEA molecule in the C2/c polymorph by increasing the lateral slip distance. The results presented here show that BPEA has a strong potential as an SF chromophore for enhancing solar cell performance.

ASSOCIATED CONTENT

* Supporting Information

Detailed sample preparation procedures, additional X-ray, fsTA, nsTA, kinetic modeling, and computational data (PDF)

AUTHOR INFORMATION

Corresponding Author

*m-wasielewski@northwestern.edu

ORCID

Gyeongwon Kang: 0000-0002-8219-2717

Christos D. Malliakas: 0000-0003-4416-638X

Jiawang Zhou: 0000-0002-2399-0030

Ryan M. Young: 0000-0002-5108-0261

Yi-Lin Wu: 0000-0003-0253-1625

Richard P. Van Duyne: 0000-0001-8861-2228

George C. Schatz: 0000-0001-5837-4740

Michael R. Wasielewski: 0000-0003-2920-5440

Notes

The authors declare no competing financial interest.

ACKNOWLEDGMENTS

This work was supported by the U.S. Department of Energy, Office of Science, Office of Basic Energy Sciences under Award DE-FG02-99ER14999 (M.R.W., experiments) and by the National Science Foundation under grant no. CHE-1760537 (G.C.S., theory). G.K., R.P.V.D., and G.C.S. acknowledge support from the Air Force Office of Scientific Research MURI (FA9550-14-1-0003, theory). We thank Dr. Eileen Foszcz for her assistance with the 100 kHz fsTA measurements.

REFERENCES

(1) Singh, S.; Jones, W. J.; Siebrand, W.; Stoicheff, B. P.; Schneider, W. G. Laser Generation of Excitons and Fluorescence in Anthracene Crystals. J. Chem. Phys. 1965, 42, 330−342.

(2) Smith, M. B.; Michl, J. Singlet Fission. Chem. Rev. 2010, 110, 6891−6936.

(3) Hanna, M. C.; Nozik, A. J. Solar Conversion Efficiency of Photovoltaic and Photoelectrolysis Cells with Carrier Multiplication Absorbers. J. Appl. Phys. 2006, 100, 074510.

(4) Lee, J.; Jadhav, P.; Reusswig, P. D.; Yost, S. R.; Thompson, N. J.; Congreve, D. N.; Hontz, E.; Van Voorhis, T.; Baldo, M. A. Singlet Exciton Fission Photovoltaics. Acc. Chem. Res. 2013, 46, 1300−1311.

(5) Rao, A.; Friend, R. H. Harnessing Singlet Exciton Fission to Break the Shockley-Queisser Limit. Nat. Rev. Mater. 2017, 2, 17063.

(6) Piland, G. B.; Burdett, J. J.; Dillon, R. J.; Bardeen, C. J. Singlet Fission: From Coherences to Kinetics. J. Phys. Chem. Lett. 2014, 5, 2312−2319.

(7) Dexter, D. L. Two Ideas on Energy Transfer Phenomena: Ion-Pair Effects Involving the Oh Stretching Mode, and Sensitization of Photovoltaic Cells. J. Lumin. 1979, 18−19, 779−784.

(8) Thompson, N. J.; Wilson, M. W. B.; Congreve, D. N.; Brown, P. R.; Scherer, J. M.; Bischof, T. S.; Wu, M.; Geva, N.; Welborn, M.; Voorhis, T. V.; Bulović, V.; Bawendi, M. G.; Baldo, M. A. Energy Harvesting of Non-Emissive Triplet Excitons in Tetracene by Emissive Pbs Nanocrystals. Nat. Mater. 2014, 13, 1039−1043.

(9) Tabachnyk, M.; Ehrler, B.; Gelinas, S.; Böhm, M. L.; Walker, B. J.; Musselman, K. P.; Greenham, N. C.; Friend, R. H.; Rao, A. Resonant Energy Transfer of Triplet Excitons from Pentacene to Pbse Nanocrystals. Nat. Mater. 2014, 13, 1033−1038.

(10) Congreve, D. N.; Lee, J.; Thompson, N. J.; Hontz, E.; Yost, S. R.; Reusswig, P. D.; Bahlke, M. E.; Reineke, S.; Van Voorhis, T.; Baldo, M. A. External Quantum Efficiency above 100% in a Singlet-Exciton-Fission-Based Organic Photovoltaic Cell. Science 2013, 340, 334−337.

(11) Kim, H.; Keller, B.; Ho-Wu, R.; Abeyasinghe, N.; Vazquez, R. J.; Goodson, T.; Zimmerman, P. M. Enacting Two-Electron Transfer from a Double-Triplet State of Intramolecular Singlet Fission. J. Am. Chem. Soc. 2018, 140, 7760−7763.

(12) Shockley, W.; Queisser, H. J. The Shockley-Queisser Limit. J. Appl. Phys. 1961, 32, 510−519.

(13) Lee, J.; Bruzek, M. J.; Thompson, N. J.; Sfeir, M. Y.; Anthony, J. E.; Baldo, M. A. Singlet Exciton Fission in a Hexacene Derivative. Adv. Mater. 2013, 25, 1445−1448.
(14) Swager, T. M.; Gil, C. J.; Wrighton, M. S. Fluorescence Studies of Poly(p-phenyleneethynylene)s: The Effect of Anthracene Sub-stitution. J. Phys. Chem. 1995, 99, 4886−4893.
(15) Gimenez, R.; Piñol, M.; Serrano, J. L. Luminescent Liquid Crystals Derived from 9,10-Bis(phenylethynyl)anthracene. Chem. Mater. 2004, 16, 1377−1383.
(16) Hanhela, P. J.; Paul, D. B. Evaluation of Fluorescent Materials for Colour Control of Peroxylate Chemiluminescence. IV Fluorescence Quantum Yields of Some Phenyl and Phenylethynyl Aromatic Compounds. Aust. J. Chem. 1984, 37, 553−559.
(17) Wang, C.; Liu, Y.; Wei, Z.; Li, H.; Xu, W.; Hu, W. Biphase Micro/Nanometer Sized Single Crystals of Organic Semiconductors: Control Synthesis and Their Strong Phase Dependent Optoelectronic Properties. Appl. Phys. Lett. 2010, 96, 143302.
(18) Zhao, Y. S.; Xu, J.; Peng, A.; Fu, H.; Ma, Y.; Jiang, L.; Yao, J. Optical Waveguide Based on Crystalline Organic Microtubes and Microrods. Angew. Chem., Int. Ed. 2008, 47, 7301−7305.
(19) Valentini, L.; Bagnis, D.; Marrocchi, A.; Seri, M.; Taticchi, A.; Kenny, J. M. Novel Anthracene-Core Molecule for the Development of Efficient PCBM-Based Solar Cells. Chem. Mater. 2008, 20, 32−34.
(20) Mitsui, M.; Kawano, Y.; Takahashi, R.; Fukui, H. Photophysics and Photostability of 9,10-Bis(phenylethynyl)anthracene Revealed by Single-Molecule Spectroscopy. RSC Adv. 2012, 2, 9921−9931.
(21) Levitus, M.; Garcia-Garibay, M. A. Polarized Electronic Spectroscopy and Photophysical Properties of 9,10-Bis-(phenylethynyl)anthracene. J. Phys. Chem. A 2000, 104, 8632−8637.
(22) Lübtow, M.; Helmers, I.; Stepanenko, V.; Albuquerque, R. Q.; Marder, T. B.; Fernández, G. Self-Assembly of 9,10-Bis-(phenylethynyl) Anthracene (BPEA) Derivatives: Influence of π-π and Hydrogen-Bonding Interactions on Aggregate Morphology and Self-Assembly Mechanism. Chem. - Eur. J. 2017, 23, 6198−6205.
(23) Manna, B.; Nandi, A.; Ghosh, R. Ultrafast Singlet Exciton Fission Dynamics in 9,10-Bis(phenylethynyl)anthracene Nanoaggregates and Thin Films. J. Phys. Chem. C 2018, 122, 21047−21055.
(24) Pun, J. K. H.; Gallaher, J. K.; Frazer, L.; Prasad, S. K. K.; Dover, C. B.; MacQueen, R. W.; Schmidt, T. W. TIPS-Anthracene: A Singlet Fission or Triplet Fusion Material? J. Photonics Energy 2018, 8, 022006.
(25) Rietveld, H. A Profile Refinement Method for Nuclear and Magnetic Structures. J. Appl. Crystallogr. 1969, 2, 65−71.
(26) Nguyen, P.; Todd, S.; Vandenbiggelaar, D.; Taylor, N. J.; Marder, T. B.; Wittmann, F.; Friend, R. H. Facile Route to Highly Fluorescent 9,10-Bis(p-R-phenylethynyl)anthracene Chromophores via Palladium-Copper Catalyzed Cross-Coupling. Synlett 1994, 1994, 299−301.
(27) Demeter, A. First Steps in Photophysics. I. Fluorescence Yield and Radiative Rate Coefficient of 9,10-Bis(phenylethynyl)anthracene in Paraffins. J. Phys. Chem. A 2014, 118, 9985−9993.
(28) Hestand, N. J.; Spano, F. C. Molecular Aggregate Photophysics Beyond the Kasha Model: Novel Design Principles for Organic Materials. Acc. Chem. Res. 2017, 50, 341−350.
(29) Vincett, P. S.; Voigt, E. M.; Rieckhoff, K. E. Phosphorescence and Fluorescence of Phthalocyanines. J. Chem. Phys. 1971, 55, 4131− 4140.
(30) Rihter, B. D.; Kenney, M. E.; Ford, W. E.; Rodgers, M. A. J. Synthesis and Photoproperties of Diamagnetic Octabutoxyphthalo-cyanines with Deep Red Optical Absorbance. J. Am. Chem. Soc. 1990, 112, 8064−8070.
(31) Margulies, E. A.; Logsdon, J. L.; Miller, C. E.; Ma, L.; Simonoff, E.; Young, R. M.; Schatz, G. C.; Wasielewski, M. R. Direct Observation of a Charge-Transfer State Preceding High-Yield Singlet Fission in Terrylenediimide Thin Films. J. Am. Chem. Soc. 2017, 139, 663−671.
(32) Walker, B. J.; Musser, A. J.; Beljonne, D.; Friend, R. H. Singlet Exciton Fission in Solution. Nat. Chem. 2013, 5, 1019−1024.
(33) Burdett, J. J.; Bardeen, C. J. The Dynamics of Singlet Fission in Crystalline Tetracene and Covalent Analogs. Acc. Chem. Res. 2013, 46, 1312−1320.
(34) Eaton, S. W.; Shoer, L. E.; Karlen, S. D.; Dyar, S. M.; Margulies, E. A.; Veldkamp, B. S.; Ramanan, C.; Hartzler, D. A.; Savikhin, S.; Marks, T. J.; Wasielewski, M. R. Singlet Exciton Fission in Polycrystalline Thin Films of a Slip-Stacked Perylenediimide. J. Am. Chem. Soc. 2013, 135, 14701−14712.
(35) Le, A. K.; Bender, J. A.; Arias, D. H.; Cotton, D. E.; Johnson, J. C.; Roberts, S. T. Singlet Fission Involves an Interplay between Energetic Driving Force and Electronic Coupling in Perylenediimide Films. J. Am. Chem. Soc. 2018, 140, 814−826.
(36) Nichols, V. M.; Broch, K.; Schreiber, F.; Bardeen, C. J. Excited-State Dynamics of Diindenoperylene in Liquid Solution and in Solid Films. J. Phys. Chem. C 2015, 119, 12856−12864.
(37) Carmichael, I.; Hug, G. L. Triplet−Triplet Absorption Spectra of Organic Molecules in Condensed Phases. J. Phys. Chem. Ref. Data 1986, 15, 1−250.
(38) Sanders, S. N.; Kumarasamy, E.; Pun, A. B.; Trinh, M. T.; Choi, B.; Xia, J.; Taffet, E. J.; Low, J. Z.; Miller, J. R.; Roy, X.; Zhu, X. Y.; Steigerwald, M. L.; Sfeir, M. Y.; Campos, L. M. Quantitative Intramolecular Singlet Fission in Bipentacenes. J. Am. Chem. Soc. 2015, 137, 8965−8972.
(39) Hartnett, P. E.; Margulies, E. A.; Mauck, C. M.; Miller, S. A.; Wu, Y.; Wu, Y.-L.; Marks, T. J.; Wasielewski, M. R. Effects of Crystal Morphology on Singlet Exciton Fission in Diketopyrrolopyrrole Thin Films. J. Phys. Chem. B 2016, 120, 1357−1366.
(40) Eaton, S. W.; Miller, S. A.; Margulies, E. A.; Shoer, L. E.; Schaller, R. D.; Wasielewski, M. R. Singlet Exciton Fission in Thin Films of tert-Butyl-substituted Terrylenes. J. Phys. Chem. A 2015, 119, 4151−4161.
(41) Mauck, C. M.; Hartnett, P. E.; Margulies, E. A.; Ma, L.; Miller, C. E.; Schatz, G. C.; Marks, T. J.; Wasielewski, M. R. Singlet Fission via an Excimer-Like Intermediate in 3,6-Bis(Thiophen-2-yl)-Diketopyrrolopyrrole Derivatives. J. Am. Chem. Soc. 2016, 138, 11749−11761.
(42) Berkelbach, T. C.; Hybertsen, M. S.; Reichman, D. R. Microscopic Theory of Singlet Exciton Fission. II. Application to Pentacene Dimers and the Role of Superexchange. J. Chem. Phys. 2013, 138, 114103.
(43) Miller, C. E.; Wasielewski, M. R.; Schatz, G. C. Modeling Singlet Fission in Rylene and Diketopyrrolopyrrole Derivatives: The Role of the Charge Transfer State in Superexchange and Excimer Formation. J. Phys. Chem. C 2017, 121, 10345−10350.
(44) Buchanan, E. A.; Havlas, Z.; Michl, J. Singlet Fission: Optimization of Chromophore Dimer Geometry. Adv. Quantum Chem. 2017, 75, 175−227.
(45) Da Silva Filho, D. A.; Kim, E. G.; Bredas, J. L. Transport Properties in the Rubrene Crystal: Electronic Coupling and Vibrational Reorganization Energy. Adv. Mater. 2005, 17, 1072−1076.
(46) Renaud, N.; Sherratt, P. A.; Ratner, M. A. Mapping the Relation between Stacking Geometries and Singlet Fission Yield in a Class of Organic Crystals. J. Phys. Chem. Lett. 2013, 4, 1065−1069.
(47) Arias, D. H.; Ryerson, J. L.; Cook, J. D.; Damrauer, N. H.; Johnson, J. C. Polymorphism Influences Singlet Fission Rates in Tetracene Thin Films. Chem. Sci. 2016, 7, 1185−1191.